https://ntrs.nasa.gov/search.jsp?R=20140008747 2019-08-29T13:55:55+00:00Z

AAS 14-051

SPACE LAUNCH SYSTEM IMPLEMENTATION OF ADAPTIVE AUGMENTING CONTROL

John H. Wall*

Jeb S. Orr†

Tannen S. VanZwieten‡

Given the complex structural dynamics, challenging ascent performance requirements, and rigorous flight certification constraints owing to its manned capability, the NASA Space Launch System (SLS) launch vehicle requires a proven thrust vector control algorithm design with highly optimized parameters to provide stable and high-performance flight. On its development path to Preliminary Design Review (PDR), the SLS flight control system has been challenged by significant vehicle flexibility, aerodynamics, and sloshing propellant. While the design has been able to meet all robust stability criteria, it has done so with little excess margin. Through significant development work, an Adaptive Augmenting Control (AAC) algorithm has been shown to extend the envelope of failures and flight anomalies the SLS control system can accommodate while maintaining a direct link to flight control stability criteria such as classical gain and phase margin. In this paper, the work performed to mature the AAC algorithm as a baseline component of the SLS flight control system is presented. The progress to date has brought the algorithm design to the PDR level of maturity. The algorithm has been extended to augment the full SLS digital 3-axis autopilot, including existing load-relief elements, and the necessary steps for integration with the production flight software prototype have been implemented. Several updates which have been made to the adaptive algorithm to increase its performance, decrease its sensitivity to expected external commands, and safeguard against limitations in the digital implementation are discussed with illustrating results. Monte Carlo simulations and selected stressing case results are also shown to demonstrate the algorithm's ability to increase the robustness of the integrated SLS flight control system.

1 INTRODUCTION

Space Launch System (SLS), currently in development by NASA, is an exploration-class launch vehicle which harnesses the experience gained through more than fifty years of United States rocket development. The SLS vehicles in their various configurations will provide access to a wide array of space destinations ranging from the International Space Station (ISS) in low earth orbit (LEO), the Moon, Mars, and near-earth asteroids. Space Launch System is a scalable launch vehicle architecture, and supports a variety of payload classes enabling unprecedented mission capability.

*Engineer, Guidance, Navigation, and Control Group; Dynamic Concepts, Inc. (Jacobs ESSSA Group), Huntsville, AL, 35806

†Senior Member of the Technical Staff, Dynamics and Control; The Charles Stark Draper Laboratory, Inc. (Jacobs ESSSA Group), Huntsville, Alabama, 35806

‡Aerospace Engineer, Control Systems Design and Analysis Branch, NASA Marshall Space Flight Center, AL, 35812

The SLS flight control system is designed to be scalable, extensible, and exceptionally robust in light of its application to a manned system. Its design maintains simplicity in an attempt to minimize the cost and complexity associated with certification of new algorithms and software. Using a design philosophy firmly anchored to proven analysis methods, coupled with an incremental test and evaluation approach for new technology risk reduction, new capabilities are being demonstrated that are novel for a manned space launcher. The design philosophy and flight certification processes associated with the integrated launch vehicle are discussed extensively elsewhere.[1] Herein, the implementation of one such technology, the adaptive augmenting control (AAC) algorithm, is detailed.

The adaptive augmenting control algorithm implemented for Space Launch System is an extension of the work originally presented by Orr and VanZwieten and developed under NASA funding near the end of the Constellation program.[2] The AAC algorithm was originally architected with three fundamental design objectives. The first objective is to adapt minimally when the baseline control system is performing acceptably. The second objective is to increase the performance and command tracking when extreme off nominal conditions and disturbances produce large errors. The third and final objective is to decrease the system gain to suppress or stabilize undesirable high frequency content in the control path. Figure 1 shows the conceptual regions of operation for adaptive control, illustrating the idea behind the first objective as compared to the second and third.

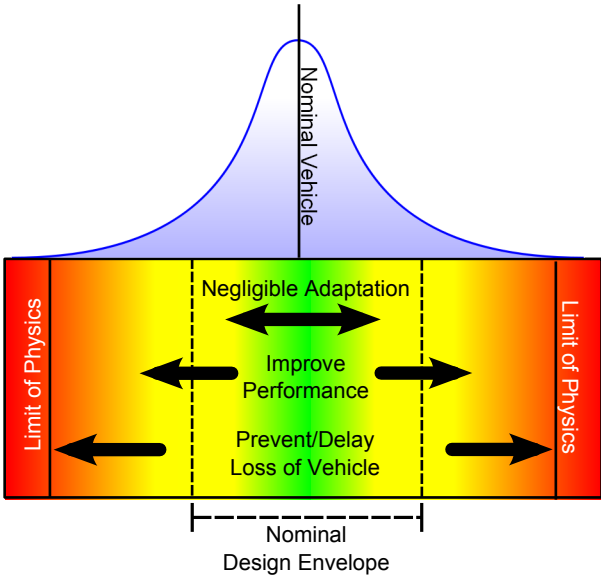

Figure 1. Conceptual Regions of Operation for Adaptive Augmentation

The theoretical development and initial simulation implementation of AAC demonstrated real and tangible benefits in physically realistic launch vehicle failure scenarios. Development of the AAC continued including its test and evaluation for the SLS launch vehicle. Simulation analyses conducted prior to SLS PDR conclusively demonstrated the value of limited-authority adaptation in mitigating the effects of environmental and vehicle model uncertainty as well as specific, generally catastrophic, failure modes associated with major launch vehicle component anomalies. Extensive development and simulation testing was conducted, primarily with the goal of integrating the adaptive algorithm into a robust and reconfigurable flight software implementation. Finally, with support from the NASA Engineering Safety Center (NESC), the NASA Space Technology Mission Directorate, and the Game Changing Development program, a flight test campaign was undertaken as

a risk reduction exercise using a surrogate F/A-18 aircraft at the NASA Dryden Flight Research Center (DFRC). This was referred to as Launch Vehicle Adaptive Control (LVAC) project. Detailed results from the flight test are discussed in a companion paper.[3]

The structure of this paper is as follows. Section 2 summarizes the basic function of the adaptive gain law. Section 3 details its integration with the baseline, gain-scheduled flight control algorithm. Section 4 presents simulation results and Section 5 concludes with final remarks.

2 ADAPTIVE GAIN LAW

Through continued development of the adaptive gain algorithm during SLS GN&C design cycles and during preparation for the LVAC flight tests, the basic form of the adaptive gain law was modified in a few respects since its original formulation. The basic form of the original adaptive gain law is repeated here in Equation 1.

$$\dot{k}_a = \left(\frac{k_{max} - k_a}{k_{max}}\right) a e_r^2 - \alpha k_a y_s - \beta(k_T - 1) \tag{1}$$

The total loop gain, shown in Figure 2, is computed as $k_T = k_0 + k_a$ where k_0 and k_{max} are the minimum total loop gain and maximum adaptation gains, respectively. The reference model error is e_r, the spectral damper input is y_s, and a, α, β are the adaptive error gain, spectral damper gain, and leakage gain, respectively. The reference model error input causes an adaptation gain increase enabling the adaptive controller to meet Objective 2 such as when large off-nominal disturbances are present. The spectral input decreases the adaptive gain in order to suppress higher frequency parasitic modes and meet Objective 3. The third term on the right hand side of Equation 1 provides leakage functionality which serves to attract the gain back to its nominal gain-scheduled value in the absence of external excitation (first-order decay), thus meeting Objective 1.

The modified formulation of the adaptive gain law as currently implemented in the SLS flight control system is shown below in Equation 2.

$$\dot{k}_T = p_{hi}(k_T) a e_r^2 - p_{lo}(k_T) \alpha y_s - \beta(k_T - 1) \tag{2}$$

One immediately apparent reduction in complexity of the updated adaptive equation is that the nonlinear dependence on the adaptation gain k_a, has been removed from the formulation. Additionally, the adaptation law has been recast directly in terms of the total loop gain k_T. The removal of k_a from the right hand side reduces the nonlinearity in the adaptation gain response, simplifying analysis of its dynamic behavior and allows for a more rapid response to error. The terms $p_{hi}(k_T)$ and $p_{lo}(k_T)$ are nonlinear saturation functions allowing further tunability and are discussed in Section 3.

The AAC reference model and spectral damper filters begin execution, along with the flight control system, at booster ignition. The adaptive law integration is inhibited until after the vehicle is clear of the ground support equipment and the initial pitch-over to start the gravity turn has been initiated. All adaptive law parameters are scheduled as a function of mission elapsed time, whereas many of the flight control system parameters during boost phase are tabulated against navigated relative velocity. Since AAC parameter variations along the trajectory have not been necessary, the use of time has been shown to be acceptable as an independent variable.

Figure 2 shows a conceptual block diagram of the SLS flight control system with AAC.

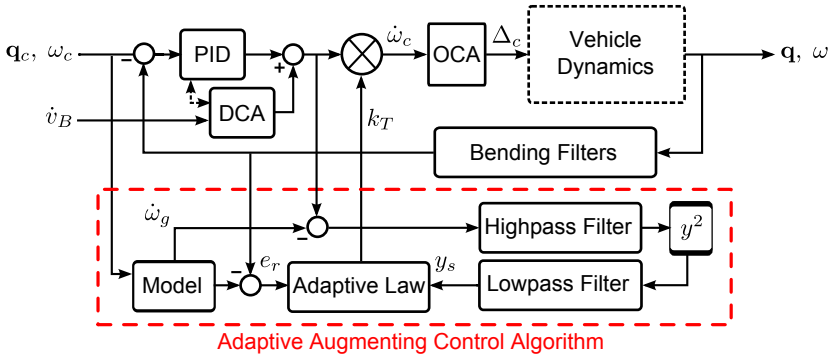

Figure 2. Block Diagram of SLS FCS with AAC

3 APPLICATION TO BASELINE CONTROL LAW

The SLS flight control system outputs commands in terms of angular acceleration for both numerical and practical convenience.[1] For each of the roll, pitch, and yaw control axes, a scalar angular acceleration command $\dot{\omega}_c$, is provided to the Optimal Control Allocator (OCA), which in turn commands individual engine actuator positions Δ_c, using a pseudo-optimal linear allocation scheme. The total angular acceleration command in each axis is computed as a function of several inputs. The pitch axis angular acceleration command is given by (other axes are identical)

$$\dot{q}_c = k_T \left(k_p \theta_e + k_d q_e + \int_{t_0}^{t_0+t} k_i \theta_e d\tau + \dot{q}_{DCA} \right) + \dot{q}_{PTI} \tag{3}$$

where k_p, k_d, and k_i are the proportional, derivative, and integral gains, and θ_e and q_e are the filtered angular errors and angular rate errors, respectively. The quantity $\dot{q}_{DCA}$, is the angular acceleration bias commanded by the Disturbance Compensation Algorithm (DCA) to counter unexpected moments,[1] and $\dot{q}_{PTI}$ is the angular acceleration programmed test input (PTI) employed during flight tests for system identification. The first four terms are modulated by the total gain k_T, which is adjusted by the adaptive algorithm. The PTI is not adjusted by the total gain since it is an open loop signal derived from a look-up table. Inclusion of the disturbance compensation signal in the modulated command path aids the performance in Objective 2 scenarios as its disturbance rejection bandwidth is proportionally increased by the total gain. The single angular acceleration command path $\dot{\omega}_c$, is the point in the system at which the single-input, single-output (SISO) open loop system response is computed; gain modulation at this point intuitively adjusts the forward gain of the entire open loop transfer function.

3.1 Reference Model Architecture

The adaptive control error signals are generated via comparison of the plant's measured dynamics with a linear, time-varying model that provides a reference for the expected behavior of the vehicle dynamics. Initial studies made the assumption that a model-reference architecture would necessitate a relatively high-fidelity dynamic model of the closed-loop system in order to generate an accurate error signal. The initial design of the reference model included elements such as the translation states of the vehicle with respect to the trajectory (in order to capture short period effects of angle-of-attack and sideslip perturbations), the actuator dynamics, and a full model of the autopilot including

bending filters. It was deemed through analysis and simulation that the additional complexity was not warranted and a simpler reference model architecture was employed.

Independently propagated for the roll, pitch, and yaw axes, the reference model used in the present formulation is an explicitly discretized, second-order, linear parameter varying filter that approximates the desired closed-loop dynamics with a natural frequency, damping ratio, and delay that varies according to a prescribed schedule as a function of flight condition. The reference model output depends on the measured quaternion error $\mathbf{q}_e$ (representing the eigenaxis rotation from the commanded inertial attitude to the measured vehicle attitude), the current guidance command quaternion $\mathbf{q}_c$, the commanded attitude rate ω_c, and the reference proportional and derivative gains k_{pr} and k_{dr}.

The approximation of the closed loop vehicle dynamics as a second-order system has many advantages, including the fact that analysis of the reference model behavior is straightforward and that the linear parameter-varying system has analytically predictable behavior under interpolation. The introduction of delay is necessary to capture phasing effects (especially in the response to time-varying commands) caused by the parasitic dynamics in the real system. It is sufficient to adjust the delay parameter to effect adequate matching of the reference model since many of the parasitic effects that do not include true latencies (e.g. actuator and sensor dynamics) affect primarily the phase response in the region near the rigid-body control frequency. In addition, most guidance commands are, by design, band-limited to reduce adverse excitation of the vehicle actuators and structure.

It was considered in the development of the reference model that the adaptive law itself is low-pass, and thus model error dynamics having a period shorter than about two seconds are, by design, ignored. Figure 3 shows the roll, pitch, yaw rate responses from the vehicle and the AAC reference model demonstrating acceptable agreement between the simplified model and actual vehicle response to guidance commands. Note that each of the figures is shown on a different scale with roll experiencing the largest commands during the region prior to maximum dynamic pressure, pitch showing second highest commands including the tower avoidance maneuver and gravity turn with adjustments based on day-of-launch wind measurements, and the yaw axis showing minimal commands except for some cross-axis coupling during the larger vehicle maneuvers.

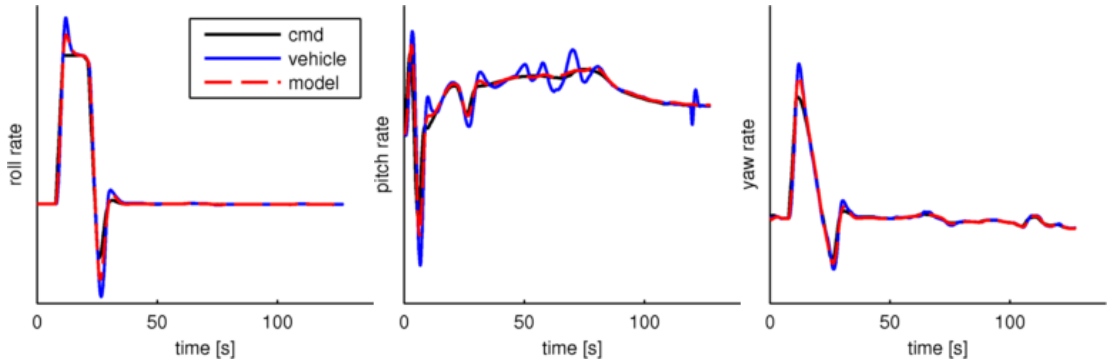

Figure 3. Command and response of vehicle and AAC reference model: Roll Axis

The reference model propagates an estimate of the transient attitude kinematics that is used to compute the trajectory-relative model error. Quaternion algebra is used to generate an expected (reference) quaternion error $\hat{\mathbf{q}}_e$, and since the reference model restoring acceleration is a linear function of the trajectory-relative error and error rate, each axis has the required low-pass filter

characteristic. Let $f_{\Theta\mathbf{q}} : \mathbb{R}^4 \rightarrow \mathbb{R}^3$ be the nonlinear mapping of a quaternion to a (3,2,1) Euler angle sequence, and let $\Theta_e = f_{\Theta\mathbf{q}}(\mathbf{q}_e)$ and $\hat{\Theta}_e = f_{\Theta\mathbf{q}}(\hat{\mathbf{q}}_e)$.

The error signal generated for the adaptive control law is

$$e_r = c\left(\Theta_e - \hat{\Theta}_e\right) + \omega_e - \hat{\omega}_e \tag{4}$$

where Θ_e is the Euler angle error associated with the eigenaxis rotation from vehicle navigated quaternion (filtered) to guidance-commanded quaternion, $\hat{\Theta}_e$ is the Euler angle error computed in the reference model, and ω_e, $\hat{\omega}_e$ are the filtered, measured body angular rate and the reference model angular rate errors, respectively. Assuming for the purposes of discussion that the errors are small,

$$\begin{aligned}
\Theta_e &= \Theta_c - \Theta \\
\hat{\Theta}_e &= \Theta_c - \hat{\Theta} \\
\omega_e &= \omega_c - \omega \\
\hat{\omega}_e &= \omega_c - \hat{\omega};
\end{aligned} \tag{5}$$

thus,

$$\Theta_e - \hat{\Theta}_e = \hat{\Theta} - \Theta = \gamma_r \tag{6}$$

and

$$\omega_e - \hat{\omega}_e = \hat{\omega} - \omega = \dot{\gamma}_r. \tag{7}$$

Therefore, the computed reference model error is given by the weighted linear combination of the propagated difference in the kinematic angles and body angular rates of the reference and measured vehicles, respectively. The choice of the weighting factor c in Equation 4 is influenced by the desired convergence dynamics of the actual vehicle to the reference vehicle. While the adaptive law *per se* does not act directly to reduce the reference model error e_r, a consequence of transient high-gain control in response to a large e_r is to drive the vehicle states to the reference trajectory and thus e_r toward zero. The reference model tracking error is

$$e_r = c\gamma_r + \dot{\gamma}_r, \tag{8}$$

and in the high-gain mode of operation the error dynamics are approximately governed by

$$\dot{\gamma}_r = -c\gamma_r \tag{9}$$

which converges asymptotically to zero with time constant $1/c$. The time constant is a tunable parameter chosen to be of approximately the same order as the desired rigid body dynamics.

In terms of architecture, the 3-axis reference model is complicated by the desire to propagate the attitude kinematics in terms of a commanded and achieved quaternion. The model reference architecture is shown in Figure 4.

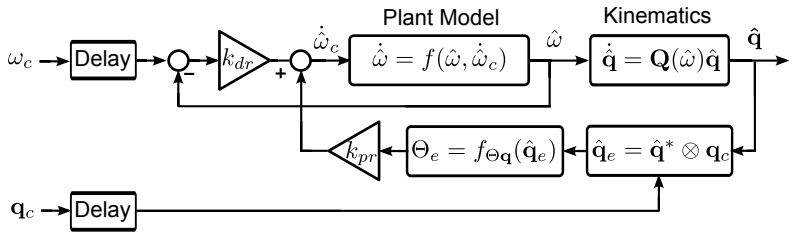

Figure 4. Reference Model Architecture

It is assumed at the outset that the model of the desired plant dynamics is a normalized integration ($\dot{\hat{\omega}} = \dot{\hat{\omega}}_c$) where $\dot{\hat{\omega}}_c$ is the commanded acceleration. The plant input commands are the commanded rate ω_c and a commanded quaternion $\mathbf{q}_c$ which is the same as that provided to the vehicle control system from the guidance and steering function. In the flight software implementation, the error $\hat{\mathbf{q}}_e$ is based upon an internally propagated estimate of the reference model kinematics as depicted in Figure 4.

However, for analysis purposes, the quaternion algebra can be linearized and partitioned into separate roll, pitch, and yaw channels. The reference model dynamics are then described by three second-order linear ordinary differential equations of the form (shown here for the pitch axis)

$$\dot{\hat{q}} = k_{pr}\left(\theta_c - \hat{\theta}\right) + k_{dr}\left(q_c - \hat{q}\right) \tag{10}$$

where θ_c, $\hat{\theta}$ are the commanded and propagated kinematic pitch angles, respectively, and q_c, $\hat{q}$ are the commanded and propagated angular pitch rates. The reference model dynamics can be written in terms of the propagated attitude state, such that

$$\ddot{\hat{\theta}} + k_{dr}\dot{\hat{\theta}} + k_{pr}\hat{\theta} = k_{pr}\theta_c + k_{dr}q_c. \tag{11}$$

In the case that the commanded rate is the time derivative of the command, the reference dynamics have the Laplace domain transfer function (with respect to commanded attitude)

$$\frac{\hat{\theta}(s)}{\theta_c(s)} = \frac{k_{pr} + k_{dr}s}{s^2 + k_{dr}s + k_{pr}}. \tag{12}$$

This second order form has natural frequency $\omega_r = \sqrt{k_{pr}}$ and damping ratio $\zeta_r = \frac{k_{dr}}{2\sqrt{k_{pr}}}$.

Finally, a variable delay is introduced in the output path, giving the response

$$H_r(s) = e^{-s\tau}\frac{\omega_r^2 + 2\zeta_r\omega_r s}{s^2 + 2\zeta_r\omega_r s + \omega_r^2}. \tag{13}$$

This characteristic is duplicated independently in all axes, and the time-varying parameters τ, ω_r, and ζ_r need not be identical.

Given a parametrization ω_r, ζ_r, the second-order form has an explicit discretization. However, integration of the nonlinear quaternion kinematics must be performed independently, so in implementation the rate dynamics are propagated using a first order discrete integration method.

3.2 Spectral Damper

The spectral damper function of the adaptive law effects a negative adaptation rate to suppress undesirable frequency content or bring unstable modes to a stable low-amplitude limit cycle. The spectral damper is constructed consistent with the original formulation in which a representative control signal is rectified to produce a signal proportional to the average power in a specified spectral band. The spectral band is determined by the choice of filter parameters of the high pass filter prior to rectification, and the power averaging window is approximately proportional to the time constant of the rectifier low-pass filter. For SLS, the parameters are selected to yield high sensitivity in the

frequency spectrum associated with propellant slosh, actuator dynamics, and structural dynamics whose adverse behavior can be suppressed or stabilized by decreasing the total loop gain.

Based upon the design presented in [2], the angular acceleration command contains information from all feedback paths and is, under nominal conditions, predictably band-limited. This command path signal is used to drive the spectral damper input. However, in the presence of rapid guidance or steering commands, the command path may contain energy at high frequencies. In order to reduce these effects, an estimate of the control command resulting from guidance inputs is subtracted from the total controller angular acceleration command prior to its injection into the spectral damper high pass filter. This correction term, $\dot{q}_g$, is derived from the reference model acceleration, given earlier in Equation 10 as

$$\dot{q}_g = \omega_r^2 \left(\theta_c - \hat{\theta}\right) + 2\zeta_r \omega_r \left(q_c - \hat{q}\right). \tag{14}$$

Additionally, the control command sent to the spectral damper in the SLS implementation is taken before the application of the gain as shown in Figure 2 which greatly reduces the propensity for adaptation induced by frequency content in the gain signal itself.

Throughout ascent flight of the SLS vehicle, optimal digital filters are applied to the error signals in order to stabilize slosh and elastic vehicle dynamics.[4] During the boost phase, due to the time-varying nature of the stressing flex and slosh dynamics, a single set of filter coefficients is insufficient to achieve robust stability design criteria. As a result, several filters are scheduled across the boost phase and the coefficients are updated at discrete points. It was discovered that the spectral damper and total adapted gain was quite sensitive to the method of filter state transitions at the coefficient update times. A revised method to re-initialize the filter states with the propagated states of the future filter yields a significantly smoother transition and eliminates the transients.

3.3 Adaptation Limits

The original adaptation formulation employed a nonlinear input saturation term on the reference model error driven signal in order to enforce smooth limiting of the adaptive gain. This nonlinear multiplier was a function of the adaptation gain itself and thus penalized the adaptation rate at high forward gains. In the modified formulation, the state-dependent saturation is replaced with a parametrized saturation function p_{hi}, given by

$$p_{hi}(k_T) = 1 - \left(1 + \exp\left[A\left(\frac{1}{A}\log\left(\frac{\epsilon k_{Tmax}}{1 - \epsilon k_{Tmax}}\right) + k_{Tmax} - k_T\right)\right]\right)^{-1}. \tag{15}$$

Where A and ϵ are parameters which define the shape of the saturation function and k_{Tmax} and k_{Tmin} are the maximum and minimum gains total gains, respectively.

The original adaptive gain law spectral damper term also included an adaptive gain multiplier. Similar to the input saturation function, the adaptation rate contribution from the spectral term would smoothly diminish as the adaptive gain decreased to its minimum value. This further ensured that the spectral damping term would never drive the adaptive gain below zero. A similar saturation function as used above replaces the k_a multiplier on the spectral damper. Like the error term multiplier, this function allows for design parametrization while continuing to ensure the adaptation rate approaches zero as the total gain reaches its minimum value. The parameterized saturation function for the lower limit is

$$p_{lo}(k_T) = \left(1 + \exp\left[A\left(\frac{1}{A}\log\left(\frac{1-\epsilon k_{Tmax}}{\epsilon k_{Tmax}}\right) + k_{Tmin} - k_T\right)\right]\right)^{-1}. \tag{16}$$

Figure 5 shows an example of saturation functions as parametrized for the SLS control law. To reduce the adaptation penalty and maintain a linear adaptation rate with respect to the error and spectral inputs, the saturation parameters have been set to provide a response which sharply diminishes the adaptation rate only when the total gain is within 5-10% of its maximum range. For SLS, the total loop gain is allowed to range from 0.5 to 2.0, corresponding to approximately -/+ 6dB, the nominal gain margin design criteria at the first two 180 deg phase crossover frequencies.

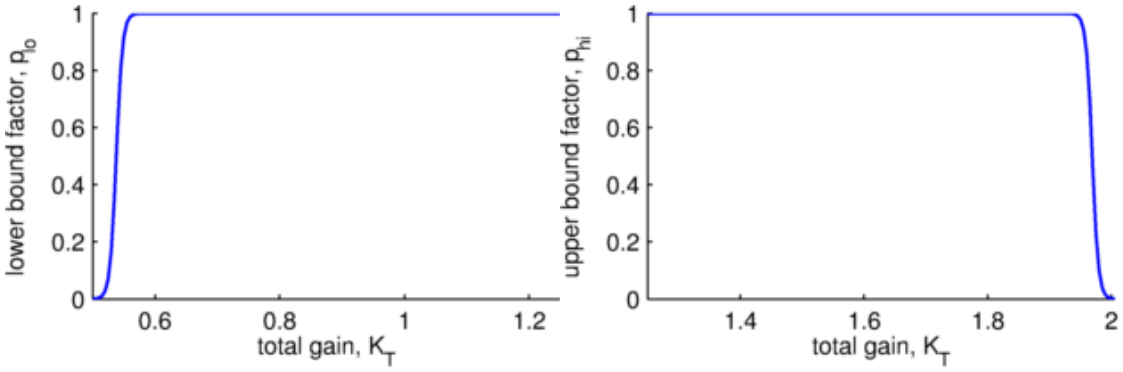

Figure 5. Adaptation Saturation Functions

The saturation functions applied to the error and spectral terms have not been shown to exhibit any adverse affects when the adaptive controller is engaged. While the saturation functions applied to the error and spectral input terms ensure that the dynamics of the total gain are analytically bounded, explicit hard limits for the total gain are additionally imposed in the flight software. These explicit limits add a layer of software protection against gain variations outside the range for which the design has been analyzed.

In addition, limits are imposed on the spectral input y_s, and the reference model error input e_r, to constrain the rate of adaptation induced by each signal. For each input, the limit for the rate of adaptation is parametrized by the time over which each term could independently result in a full scale gain change. The rate limits given in Equations 17 and 18 are derived by solving for the maximum squared reference model error or spectral damper value that would result in an adaptation rate exceeding a full range change in the specified minimum time, Δt_{elim} or Δt_{sdlim} .

$$e^2_{lim} = \left(\frac{k_{Tmax} - k_{Tmin}}{a\Delta t_{elim}}\right) \tag{17}$$

$$y_{slim} = \left(\frac{k_{Tmax} - k_{Tmin}}{\alpha\Delta t_{sdlim}}\right) \tag{18}$$

In the software implementation, the reference model error e_r^2, and spectral input y_s, are restricted to be positive. This zero lower bound is particularly important for the spectral damper as the transient response through a low pass rectifier filter having complex poles may yield negative values even when the filter input is positive.

The adaptation rate limits are essential safeguards to preclude the development of numerical integration phenomena (such as jump propagation) and to ensure that the discrete-time adaptation dynamics remain bounded in the case of large or spurious inputs.

3.4 Simulation Results

The adaptive augmenting control (AAC) algorithm has been implemented in the SLS flight software primarily to support the boost phase of flight, although plans exist to explore its extension through core stage flight. The SLS flight software, including AAC, has been evaluated in multiple time-domain simulation tools including the MSFC Crew Launch Vehicle Tree tOPology Simulation (CLVTOPS) multi-body environment and the Marshall Aerospace VEhicle Representation In C (MAVERIC) 6-DoF. A Simulink-based version of the control system software has been implemented in the companion engineering tools Stability Aerospace Vehicle ANalysis Tool (SAVANT) and NASA Langley's Space Transportation Analysis and Research Simulation (STARS), used for Verification & Validation. These independent simulation environments have been used to perform numerous Monte Carlo analyses of the boost phase of flight, during which AAC is active, and all tools have demonstrated excellent agreement of the pertinent flight mechanics metrics in nominal scenarios. The results in the following sections are representative results from the primary ascent performance analysis tool, MAVERIC. The first two sections will detail the second and third objectives of the AAC algorithm using selected stressing cases, and the third section will demonstrate the behavior of the algorithm in the mainline dispersed analysis.

3.4.1 Objective Two: Increase Performance in Off-Nominal Scenarios In the first example scenario, a combination of high winds and an aerodynamically unstable vehicle is coupled with a single core engine dual actuator hard-over which occurs during the region of maximum dynamic pressure. This extreme off-nominal scenario would normally result in a rigid body load indicator requirement violation. However, with AAC enabled, an increase in loop gain at the onset of the disturbances results in significantly better attitude tracking and as a result the rigid body load indicator stays well below the requirement.

Figure 6 shows the rigid body load indicator and the control effort with adaptive control disabled and enabled. The rigid body load indicator is the product of the dynamic pressure and the total angle of attack and provides a metric to determine the aerodynamic loads acting on the vehicle. When AAC is disabled, this stressing scenario reaches the load indicator upper limit where the plotted line terminates. With AAC enabled, the vehicle is able to better track the guidance command and avoids the angle-of-attack deviation with significant margin. The rightmost plot on Figure 6 shows the resultant control effort with and without the AAC algorithm engaged. The control effort for the fixed-gain controller reaches and remains at saturation, whereas the adaptive control briefly experiences saturation and then returns to an acceptable level of effort.

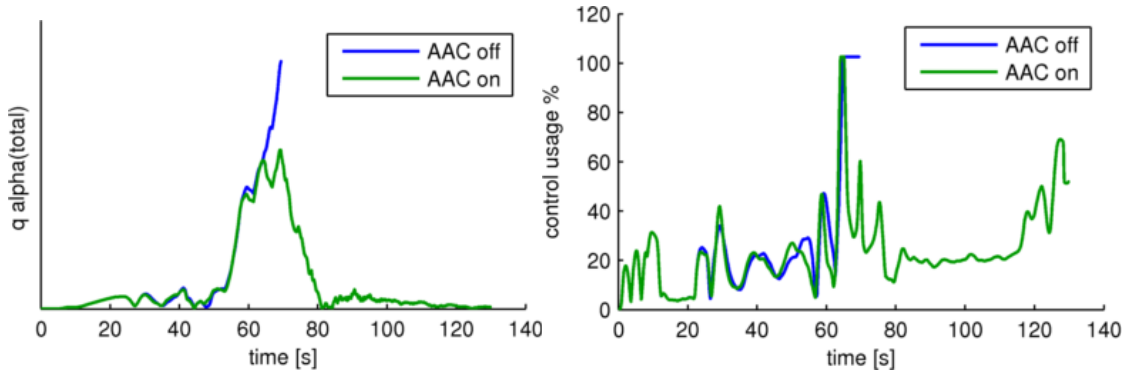

Figure 6. Objective 2 Load Indicator and Control Effort

Figure 7 depicts the total gain in the pitch (left) and yaw (right) axes, upon which the wind disturbance acts and an exaggerated aerodynamic instability is applied. The adaptive gain modulation, especially during the region of maximum dynamic pressure, results in noticeably improved command tracking.

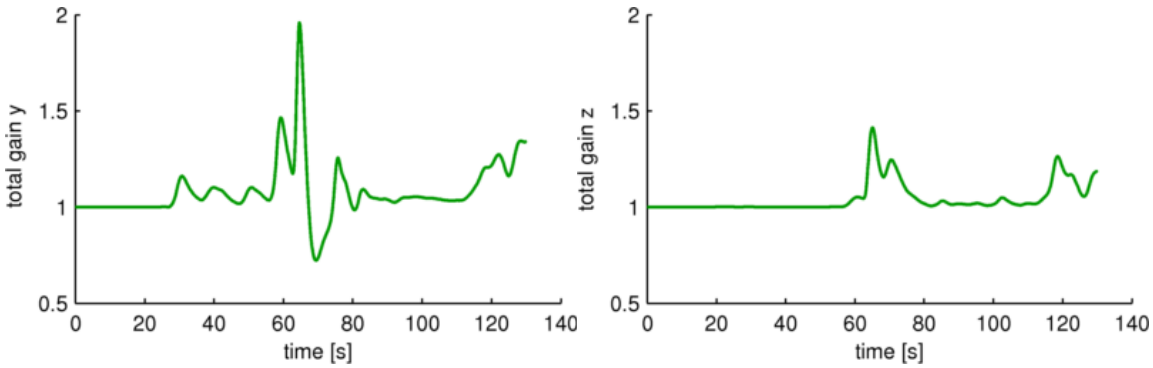

Figure 7. Objective 2 Total Gain

Figure 8 shows the guidance command relative attitude errors in pitch (left) and yaw (right). The addition of the adaptive control is very effective in reducing the significant deviations in attitude.

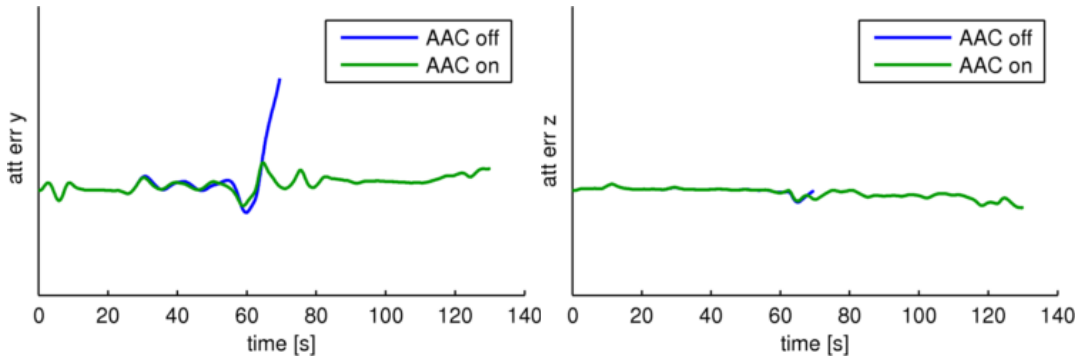

Figure 8. Objective 2 Attitude Tracking

3.4.2 Objective Three: Suppress Unstable Structural Dynamics The second example scenario demonstrates the ability of the gain adaptation to bring an otherwise unstable structural mode to a bounded limit cycle. In this particular scenario, a primary bending mode of the SLS vehicle undergoes a simulated instability during a region of flight where the gain of structural modes in the pitch and yaw axes is higher than the required critical attenuation provided by the autopilot filters.

Figure 9 shows a Bode magnitude plot of the fixed-gain open loop control response for four separate analysis times during the 50-90 second time range. The lines labeled *comp* in the plot show that the second prominent group of modes is near the critical gain (0 dB). This condition, coupled with the phasing characteristic of this particular mode, yields a potential closed-loop instability. A similar condition exists in the yaw axis and thus the resulting simulated vehicle exhibits simultaneous unstable control-structure interaction in both longitudinal axes.

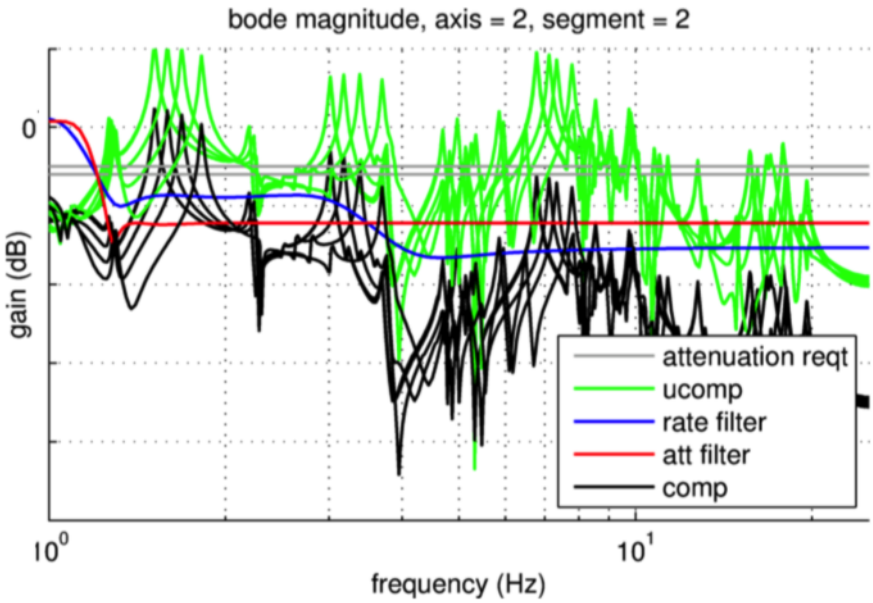

Figure 9. Objective 3 Pitch Bode Magnitude

Figure 10 shows the actuator rates of one of the thrust vectored engines throughout the boost phase for pitch (left plot) and yaw (right plot). With the fixed-gain controller (AAC off), the actuator rates grow in a divergent fashion due to the control-structure instability. At around 90 seconds, when new control filter coefficients are updated, the response decays as the updated filters sufficiently attenuate the structural resonances. With AAC enabled, the actuator rates maintain a bounded limit cycle response, reducing the actuator rates and yielding more thrust vector authority available for control.

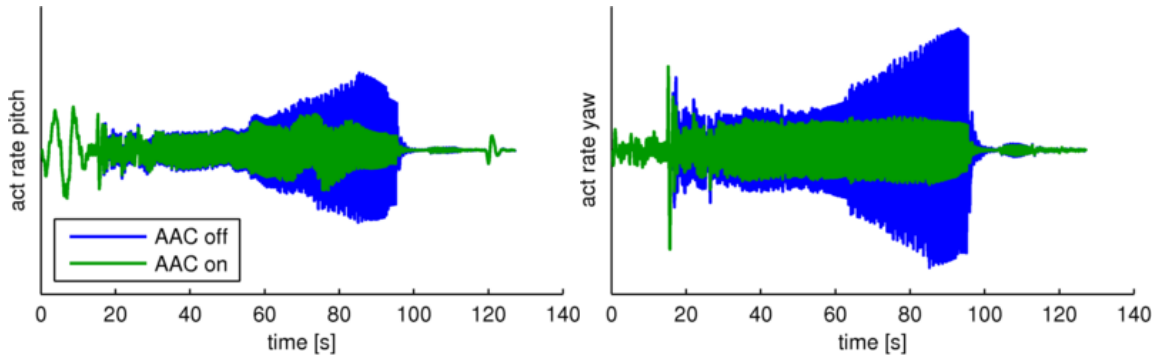

Figure 10. Objective 3 Actuator Rates

Figure 11 shows the total gain as adjusted by the AAC algorithm for pitch (left) and yaw (right). The gain decreases in each of the axes to mitigate the instability, returning back to nominal unity gain after the structural response decays.

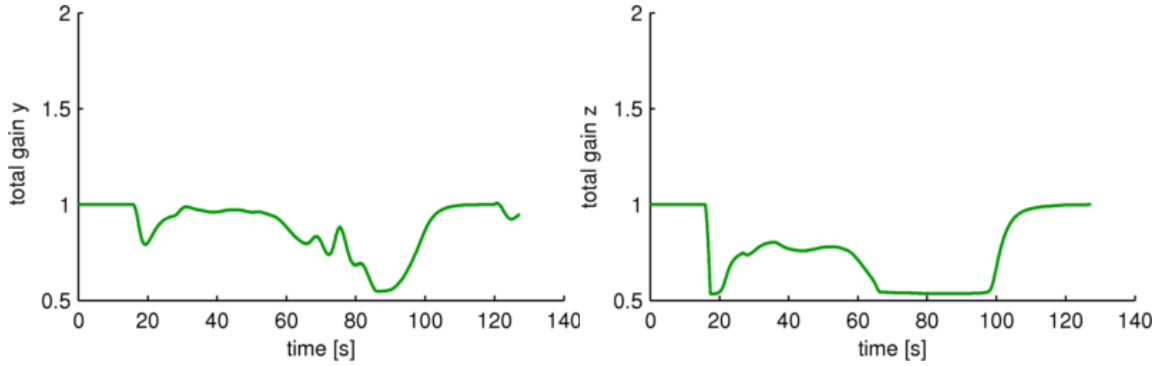

Figure 11. Objective 3 Total Gain

3.4.3 Monte Carlo Analysis Monte Carlo simulation analysis for SLS vehicle performance evaluation and requirements verification is conducted using a rigorous and extensive sampling process based upon the theory of binomial failure statistics.[5] The following results are derived from a MAVERIC 6-DOF Monte Carlo simulation ($n = 2000$) in which numerous vehicle and environment dispersions are applied. Dispersions include, but are not limited to, mass properties, aerodynamics, propellant slosh, structural flexibility, actuator dynamics, thrust misalignment, winds, and sensor errors. The results from these and similar Monte Carlo analyses have conclusively demonstrated the ability of the AAC algorithm to meet its design objectives over a wide range of off-nominal flight conditions.

Figure 12 shows the roll (x), pitch (y), and yaw (z) total gain time histories for all of the 2000 Monte Carlo runs from booster ignition (zero seconds) to booster separation. Each channel begins executing the reference model and spectral filters at booster ignition; adaptation is effective at approximately 18 seconds. The pitch axis demonstrates the least amount of adaptation throughout the ascent with total gain deviations less than $\pm 20\%$. The yaw axis similarly has minimal adaptation throughout flight with the exception of the booster tail-off region where large booster thrust imbalances impart significant yaw moments for a 5-10 second interval. The roll axis experiences the most

gain adaptation, which can be attributed to various effects corresponding to each of three regions of flight. Note that the due to the nature of the 2000 line overlay plots, it is the cases furthest from nominal which define the high ranges of the gain plots.

Throughout approximately the first third of the boost phase, the end of a relatively aggressive roll maneuver causes gain modulation as the rapid command simultaneously exaggerates the tracking error and spectral signal command compensation. The middle interval, containing the region of highest dynamic pressure, shows gain deviations commensurate with the expected errors given the challenging atmospheric flight regime. Near the end of the booster burn, a combination of thrust misalignment and side-to-side thrust tail-off dispersion induces a roll disturbance moment, increasing gain due to model tracking error. The immediate gain decreases just prior to booster separation are the result of a booster slag ejection transient conservatively modeled using Ares I-X and Shuttle flight data.

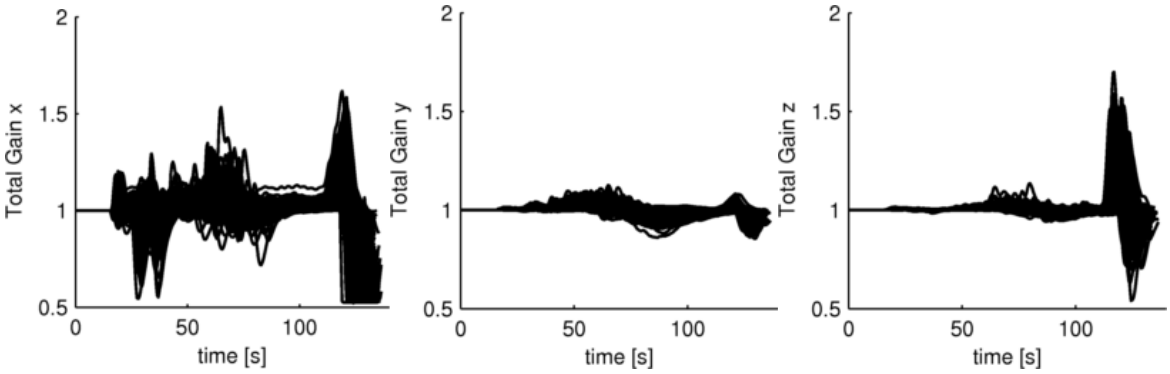

Figure 12. Total System Gain

Figure 13 shows the roll (x), pitch (y), and yaw (z) attitude errors relative to the guidance commanded trajectory. It is readily apparent from the time histories that in regions of gain increases as shown in Figure 12, the attitude tracking performance is increased. The pitch axis exhibits the best tracking (and therefore minimal adaptation) due to relatively small guidance commands during the time which AAC is active. The roll and yaw errors show a significant improvement in attitude tracking during the end of the time window when AAC is active and the larger disturbances are present.

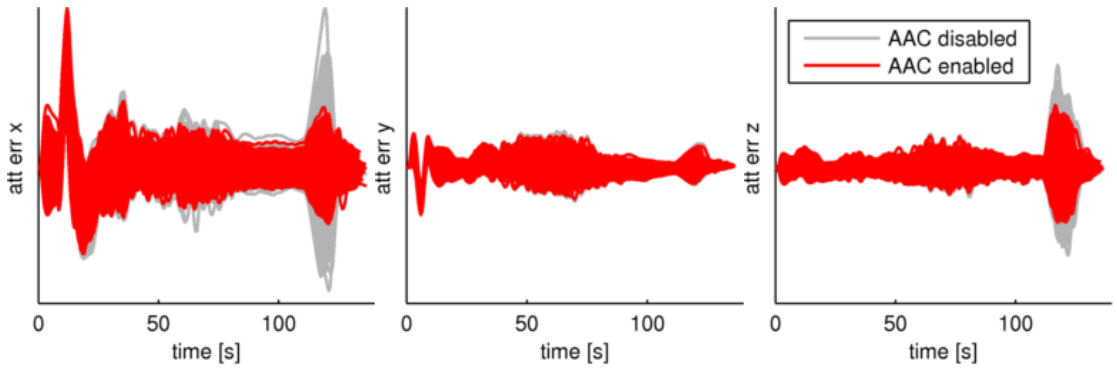

Figure 13. Attitude Errors

Figure 14 depicts the primary rigid body load indicator ($q\alpha_{total}$) (left) and the required thrust vector control authority as a percent of the total command limit (right). The envelope of both of these metrics are shown to be negligibly affected by the adaptive control gain modulation across the boost phase trajectory during which the AAC algorithm is engaged.

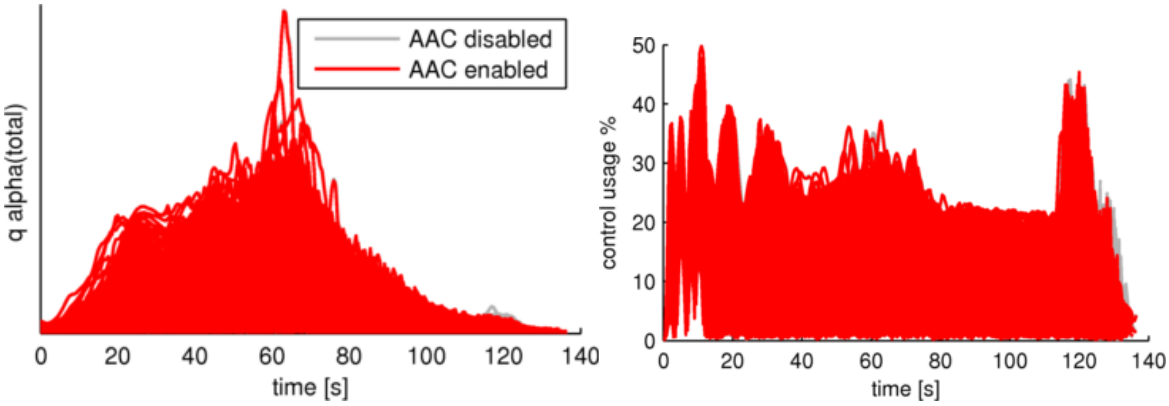

Figure 14. $q\alpha_{total}$ **Rigid Body Load Indicator and Control Usage (%)**

4 CONCLUSION

The SLS Adaptive Augmenting Control (AAC) algorithm has been successfully implemented in the Space Launch System Flight Control System software, and has been rigorously tested through extensive analysis, Monte Carlo simulation, and more recently, flight test. Several minor modifications have been made to support details specific to the integration of the algorithm in a multi-axis production launch vehicle flight software implementation as described in this paper.

ACKNOWLEDGMENTS

The authors wish to thank the members of the NASA flight controls discipline for their support of the SLS AAC project. The authors especially appreciate the contributions of Eric Gilligan, John Ottander, Charlie Hall, Don Krupp, Mark Jackson, Steve Ryan, John Hanson, and Mark West at NASA MSFC, Jim Zhu at Ohio State University, as well as the NASA DFRC LVAC engineering team, including Chris Miller, Curtis Hanson, and many others. In addition, the authors thank Neil Dennehy and Ken Lebsock of the NASA Engineering and Safety Center (NESC) and Garry Lyles, SLS Program Chief Engineer, for ongoing support of adaptive control research and its application to launch vehicles.

REFERENCES

[1] J. Orr, J. Wall, T. VanZwieten, and C. Hall, "Space Launch System Ascent Flight Control Design," in *AAS Guidance, Navigation, and Control Conference, Breckenridge, CO*, 2014. 1, 3, 3

[2] J. Orr and T. VanZwieten, "Robust, Practical Adaptive Control for Launch Vehicles," in *AIAA Guidance, Navigation, and Control Conference, Minneapolis, MN, AIAA-2012-4549*, August 2012. 1

[3] T. VanZwieten, E. Gilligan, J. Wall, and J. Orr, "Adaptive Augmenting Control Flight Characterization Experiment on an F/A-18," in *AAS Guidance, Navigation, and Control Conference, Breckenridge, CO*, 2014. 1

[4] J. Orr, "Optimal Recursive Digital Filters for Active Bending Stabilization," in *AAS Guidance, Navigation, and Control Conference, Breckenridge, CO*, 2013. 3.2

[5] J. Hanson and C. Hall, "Learning About Ares I from Monte Carlo Simulation," in *AIAA Guidance, Navigation, and Control Conference, Honolulu, HI, AIAA-2008-6622*, 2008. 3.4.3